Six-Dimensional Potential Energy Surface and Rovibrational Energies of the HCCN Radical in the Ground Electronic State†

Mirjana Mladenović* and Peter Botschwina‡

Institut für Physikalische Chemie, Universität Göttingen, Tammannstrasse 6, D-37077 Göttingen, Germany

Cristina Puzzarini||

Dipartimento di Chimica "G. Ciamician", Università di Bologna, Via Selmi 2, 40126 Bologna, Italy

Received: November 21, 2005; In Final Form: January 12, 2006

We report large-scale quantum mechanical calculations for the HCCN radical in its ground electronic state. A six-dimensional potential energy surface based on MR-ACPF/cc-pVQZ ab initio energy points is developed and adjusted to reproduce experimental findings for ν_5^1 and ν_1 of HCCN. Rovibrational energy levels of HCCN and DCCN are computed for total rotational angular momentum $J = 0-4$ by making use of combined (functional + point wise) coordinate representations together with contraction schemes resulting from several diagonalization/truncation steps. The classical barrier to linearity is determined to be 287 cm^{-1}. Spectroscopic parameters are calculated for low lying states and compared with available experimental data. Energy patterns attributed to the ν_4 bending mode and to the quasilinear ν_5 bending mode are identified. It has been also found that ν_2 and $\nu_3 + (\nu_4^1,\nu_5^1)^{0,0}$ are coupled in HCCN, while the mixing between ν_3 and $(2\nu_4^0, 2\nu_5^0)^{0,0}$ is seen in DCCN.

1. Introduction

Cyanocarbene, HCCN, has been subjected to extensive experimental[1−14] and theoretical analysis[15−22] in the last 40 years. The ground electronic state of the radical was found to have triplet multiplicity.[1−4] In the early work on HCCN, great effort was put into answering the question whether the radical is linear or bent.[1−,5,15−19] A low barrier to linearity was first estimated by theoretical means.[15−17] From a detailed microwave study of isotopically substituted HCCN, Brown et al. deduced in 1990 an unusually short CH bond length, what led to the conclusion that HCCN may possess a quasilinear structure.[5] The ν_5 fundamental transition was observed at 128.907968(40) cm^{-1} for HCCN[11] and at 2243.72708(21) GHz (74.843 cm^{-1}) for DCCN[13] by means of the far-infrared laser magnetic resonance technique. Malmquist et al.[18] and Koput[21] determined one-dimensional optimum energy profiles along the HCC angle and employed them in conjunction with the semirigid bender approach.[23] However, this model was found to be insufficient for quantitatively describing the nuclear motion in HCCN.[18,21] We refer to refs 11 and 21 for an overview of the previous experimental and theoretical studies on HCCN.

In the present paper, we have undertaken a detailed full-dimensional quantum mechanical study of HCCN and DCCN in the ground electronic state. The motivation for this work is provided by the recent high-resolution spectra[6−13] of HCCN and DCCN, which have established the frequencies of the ν_5(HCC) bending and ν_1(HC) stretching vibrations to high accuracy. The purpose of our study is to construct a potential energy surface and to compute rovibrational energy levels. Another aim is to study the quasilinear ν_5 mode under realistic conditions of the vibrating-rotating molecule and to clarify characteristic energy patterns. Our numerical results for H/DCCN are of interest for studies on tetratomic molecules involving a hydrogen atom attached to a nearly linear chain of heavy atoms, such as, e.g., HCNO, HNCO, and HNCS.

In section 2, we address the potential energy surface (PES) constructed in the present work. The computational method used to obtain rovibrational energies for $J = 0-4$ is briefly explained in section 3. Our results for HCCN and DCCN are discussed in section 4. Section 5 contains our concluding remarks.

2. Potential Energy Surface

A. Construction of the PES. The six-dimensional potential energy surface for the ground ($^3A''$) electronic state of HCCN was scanned by the multireference averaged coupled-pair-functional (MR-ACPF) method,[24−27] using the correlation consistent valence quadruple-ζ (cc-pVQZ) basis set. The Complete Active Space SCF (CASSCF) method was employed to optimize the orbitals. All calculations were performed with the MOLPRO suite of programs.[28] The nuclear coordinate space was parametrized in terms of the bond-distance-bond-angle coordinates r_1, r_2, r_3, α, β, and τ, shown in Figure 1a. Here, $r_1 = r$(H−C), $r_2 = r$(C−C), and $r_3 = r$(C−N). The two in-plane bending angles, ∠HCC and ∠CCN, are denoted respectively by α and β, whereas τ stands for the dihedral angle measured from the cis side. The PES was calculated for the region specified by $1.4a_0 < r_1 < 4.1a_0$, $1.9a_0 < r_2 < 4.6a_0$, $1.7a_0 < r_3 < 4.3a_0$, $80° \le \alpha \le 180°$, $110° \le \beta \le 180°$, and $0° \le \tau \le 180°$. In total, 1311 ab initio points were computed.

† Part of the special issue "John C. Light Festschrift".

* Corresponding author. Present address: Papendiek 17, D-37073 Göttingen, Germany. E-mail: mmladen@gwdg.de.

‡ E-mail: pbotsch@gwdg.de.

|| E-mail: cristina.puzzarini@unibo.it.

10.1021/jp056743u CCC: $33.50
Published on Web 02/18/2006

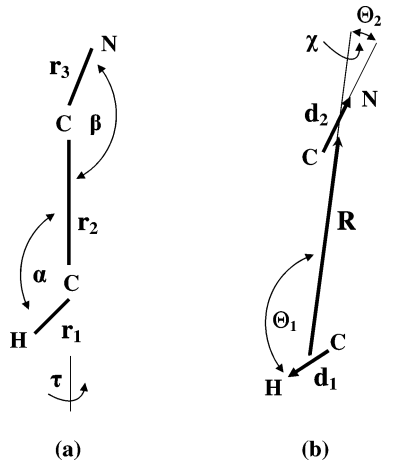

Figure 1. Description of the internal geometry of HCCN (a) in terms of the bond-distance-bond-angle internal coordinates r_1, r_2, r_3, α, β,τ and (b) in terms of the orthogonal (diatom + diatom) internal coordinates R, d_1, d_2, θ_1, θ_2, and χ.

The calculated potential energies were in the range from $-131.21429E_h$ to $-130.98376E_h$.

The ab initio points were fitted to the six-dimensional analytical expression

$$V = \sum_{ijklmn} C_{ijklmn} x_1^i x_2^j x_3^k P_l^n(c_\alpha) P_m^n(c_\beta) \cos(n\tau) \qquad (1)$$

where $c_\alpha = \cos\alpha$, $c_\beta = \cos\beta$, and l, $m \geq n$. For the stretching part, we use a polynomial expansion in the modified Morse coordinates x_i ($i = 1, 2, 3$)

$$x_i = \frac{1}{a_i}[1 - e^{-a_i(r_i/r_i^{ref}-1)}] \qquad (2)$$

recommended by Meyer et al.[29] The angular part of V is given by a multipole-like expansion, involving associated Legendre functions $P_l^n(c_\alpha)$, $P_m^n(c_\beta)$ and Chebyshev polynomials $\cos(n\tau)$, as suggested previously.[30] The functional form of eq 1 is invariant under the spatial inversion ($\tau \rightarrow 2\pi - \tau$) and independent from the torsion angle τ for linear arrangements $\alpha,\beta = 0,\pi$.

The analytical expansion of eq 1 has six nonlinear parameters, r_i^{ref} and a_i, which define the Morse coordinates x_i of eq 2. In the preliminary stages of the fitting, we employed a nonlinear least-squares technique to obtain optimum values for both r_i^{ref} and a_i. In the final fitting, r_i^{ref} and a_i were held constant. For given r_i^{ref} and a_i, the expansion parameters C_{ijklmn} were determined by means of a linear least-squares procedure.

Several sets of {i, j, k, l, m, n} were tested in our fitting of eq 1 to the ab initio points. The complete quintic expansion, augmented by the one-dimensional radial contributions up to the seventh degree and by the three-dimensional angular part of the sixth degree, was found to be sufficient for achieving a reasonable balance between the number of fitting parameters, number of input ab initio points, and associated standard deviation σ. The chosen ansatz of {i, j, k, l, m, n} defines in total 336 fitting parameters C_{ijklmn}. This number of parameters was reduced by an extensive search for all significantly determinable parameters. Eliminating stepwise all parameters smaller than twice their standard deviation and most of the parameters smaller than three times their standard deviation, we arrived at a functional six-dimensional expansion consisting of 125 terms.

TABLE 1: Expansion Coefficients C_{ijklmn} (in Atomic Units) of Eq 1 for the Adjusted Six-Dimensional MR-ACPF PES Derived in This Work for the 3A″ Electronic State of HCCN[a]

ijklmn	C_{ijklmn}	*ijklmn*	C_{ijklmn}	*ijklmn*	C_{ijklmn}
000000	−0.0000836	000310	−0.0016181	010010	0.1333863
200000	0.7423250	000020	−0.4014165	010020	0.1001659
300000	−1.2529641	000120	−0.4477221	010100	0.8068241
400000	1.2940035	000220	0.1329813	010110	1.1190861
500000	−1.1970301	000030	−0.1959100	010120	0.3713975
600000	0.9368890	000130	−0.2138155	010200	0.5152400
700000	−0.4416142	000230	0.0274065	010210	0.4998266
020000	1.2419591	000040	−0.0387080	010220	0.1619246
030000	−2.9420632	000140	−0.0431464	010300	0.0558572
040000	3.9165475	000111	0.0110927	010400	0.0233452
050000	−2.4605068	000211	0.0085826	010111	0.0762339
060000	−0.6459143	000311	0.0059613	010121	−0.0115625
002000	1.6724940	000411	−0.0010206	010211	0.0817841
003000	−5.8652217	000511	0.0003250	010311	0.0277756
004000	7.8379300	000121	0.0078587	011010	0.1585303
005000	−5.7335005	000221	0.0084313	011100	−0.2973279
006000	2.0925619	000321	0.0033287	011111	0.0491293
007000	−0.5721966	000421	−0.0004627	012100	1.4686769
011000	0.8697992	000131	0.0015849	020010	0.0403994
012000	2.0180161	000231	0.0019083	020100	−0.6353160
013000	−2.1399322	000331	0.0009184	020200	−0.5613150
014000	−2.1759310	000322	0.0003446	020300	−0.1753884
021000	−1.1684469	000422	0.0000690	020111	−0.0991483
022000	3.2219910	000232	−0.0000945	021010	0.2756852
023000	3.6368392	001010	0.5458700	021200	0.3383835
031000	−2.6150563	001020	0.5965830	030010	0.1357801
032000	−3.3335227	001030	0.1533578	030100	−0.2013531
101000	0.0217615	001100	−0.5312928	030200	−0.1253704
110000	0.0021936	001110	−0.2864925	100010	0.1117913
120000	−0.0357270	001200	−0.3406292	100020	0.0411506
201000	0.0144122	001210	−0.1293005	100100	−0.1076529
210000	0.0086634	001300	−0.0681403	100200	−0.0385778
220000	−0.1064960	001400	−0.0189303	100300	−0.0095890
000100	−0.0868363	001111	−0.0670670	100111	−0.0076520
000200	0.1745690	001211	−0.0731704	100211	−0.0051029
000300	−0.0139063	001311	−0.0235973	101100	0.0284819
000400	−0.0101806	001222	0.0016467	110100	0.0455224
000500	−0.0043744	002010	−0.7734884	200100	−0.1073827
000600	−0.0008691	002020	−0.2828110	200200	−0.0629688
000010	−0.3129661	002100	0.0868854	200300	−0.0198132
000110	−0.4723798	002111	0.0366603	300100	0.0346831
000210	0.2439514	003200	0.1573389		

[a] The reference distances $r_1^{ref} = 2.01964a_0$, $r_2^{ref} = 2.49804a_0$, and $r_3^{ref} = 2.25743a_0$ and the exponential parameters $a_1 = 0.4434$, $a_2 = 0.8009$, and $a_3 = 0.3948$ are used for the Morse coordinates x_i defined by eq 2.

For the final fitting, we set a standard deviation of a ith date point of energy E_i to be $E_i + 2000$ cm^{-1}, as previously done, e.g., by Meyer et al.[29] The standard deviation of the weighted 125-term expansion was 4.5 cm^{-1}. This σ is only 0.9 cm^{-1} larger than the σ of 3.6 cm^{-1} obtained for the initial 336-term representation. Preliminary rovibrational calculations using the 125-term PES expansion in combination with the DVR-(+R)+FBR method described below (section 3) gave the ν_1 and ν_5 fundamentals for HCCN, which deviate by 14.5 and 5.4 cm^{-1} from experiment. Our analytical representation was hence refined by adjusting the parameters C_{200000} and C_{000200} to available experimental data for the ν_1 stretching[6] and ν_5 bending[11] frequencies. The expansion coefficients C_{ijklmn} of the refined 125-term PES are listed in Table 5. The original values of C_{200000} and C_{000200} were 0.7468463 and 0.1744197, respectively.

For the equilibrium configuration, the MR-ACPF PES gives the harmonic frequencies of 3355, 1803, 1173, 553, 441, and 400 cm^{-1} for HCCN and of 2488, 1794, 1134, 506, 431, and 331 cm^{-1} for DCCN.

TABLE 2: Fundamental Transitions of HCCN and DCCN (in cm^{-1})[a]

	HCCN			DCCN		
	this work	expt	ref	this work	expt	ref
ν_1	3246.66	3246.6573(5)	6	2436.64	2436.3723(7)	9
	[25.94]	[26.80]	6	[24.44]	[25.42]	9
ν_2	1733.71	~1750	8	1730.27		
		1735	3		1729.5	3
	[49.90]			[67.84]		
ν_3	1178.57	1178.5	3	1150.65	1127	3
	[23.03]			[−9.86]		
ν_4^1	430.02	365(15)	7	407.48	367(15)	7
		383(20)	6			
		458	3		405	3
	[−20.39, −47.50]	[−21.05, −48.95]	7	[−18.36, −53.68]	[−19.07, −53.86]	7
ν_5^1	128.96	128.907968(40)	11	75.65	74.845(2)	9
		145(15)	7		90(15)	7
	[17.88, −21.98]	[18.16, −22.40]	7	[8.67, −41.12]	[8.70, −41.93]	7

[a] The number in brackets gives the difference $B_0 - B_v$ (in MHz) between the ground-state rotational constants B_0 and effective rotational constant B_v for the vibrational state v. For the MR-ACPF PES, B_0 is calculated to be 0.364872 and 0.329029 cm^{-1} for HCCN and DCCN, respectively. The corresponding experimental values due to McCarthy et al.[7] are 0.366465 and 0.330441 cm^{-1} for HCCN and DCCN, respectively.

TABLE 3: Transitions Involving the Bending ν_5 and ν_4 Vibrations[a]

	HCCN			DCCN		
	this work	expt	ref	this work	expt	ref
$2\nu_5^2$	343.44	341.73	12	210.89	207.95	12
		340(15)	7		215(15)	7
	[−27.53]	[−1.01]	7	[−32.03]	[−30.71]	7
$2\nu_5^0$	460.97	435(20)	7	317.92	311(15)	7
	[−12.86]	[−16.60]	7	[−15.91]	[−18.40]	7
$(\nu_4^1,\nu_5^1)^{0,1}$	564.77	525(20)	7	502.35		
	[−34.12]	[−35.84]	7	[−40.35]		
$(\nu_4^1,\nu_5^1)^{0,0}$	575.81	540(20)	7	516.77		
	[−26.59]	[−25.55]	7	[−107.8]		
$(\nu_4^1,\nu_5^1)^{2,p}$	560.10			495.97		
$3\nu_5^3$	618.23	625(20)	7	386.84	400(20)	7
	[−44.79]	[−2.53]	7	[−43.69]	[−43.12]	7
$3\nu_5^1$	725.75			514.90		
	[−9.43, −38.50]			[56.56, −53.20]		
$4\nu_5^4$	939.71			593.89		
$4\nu_5^2$	1007.17			697.41		
	[−45.00]			[−96.43]		
$4\nu_5^0$	1088.61			744.02		
	[−37.83]			[−58.15]		
$2\nu_4^0$	851.09			837.76		
$2\nu_4^2$	860.41			821.85		
$3\nu_4^1$	1273.46			1261.92		
$3\nu_4^3$	1290.79			1240.88		
$4\nu_4^0$	1686.79			1689.92		
$4\nu_4^2$	1695.14			1681.57		
$4\nu_4^4$	1721.89			1663.58		

[a] For more details, see Table 2.

B. Topography of the PES. The two-dimensional maps of the adjusted six-dimensional MR-ACPF PES are displayed in Figure 2. These are made by freezing the remaining four coordinates at their equilibrium values. The contour plots involving $\{\alpha,\tau\}$ and $\{\beta,\tau\}$ (the second and third plot in the second row of Figure 2) clearly show that HCCN is a planar molecule possessing only a trans minimum. The geometrical parameters of the PES minimum are given by $r_1^e = 2.020a_0$, $r_2^e = 2.499a_0$, $r_3^e = 2.257\ a_0$, $\alpha^e = 146.6°$, $\beta^e = 174.7°$, and $\tau^e = 180°$. As seen in Figure 2, the coupling between the HCC bending angle α and the CC bond length r_2 is especially prominent. Figure 2 also shows the variation of r_1, r_2, r_3, β, τ along the minimum energy path (MEP) in the direction of α, as well the variation of τ along the MEP for β. The MEP along a chosen coordinate is computed by minimizing V with respect to the remaining five coordinates. Along the MEP for α, the optimum triple (r_1, r_2, r_3) assumes the value of ($2.042a_0$, $2.565a_0$, $2.236a_0$) for $\alpha = 120°$ and of ($2.009a_0$, $2.447a_0$, $2.281a_0$) for $\alpha = 180°$, yielding changes of $-0.033a_0$, $-0.118a_0$, and $+0.045a_0$ for r_1, r_2, and r_3, respectively. Malmquist et al.[18] and Koput[21] also found that the straightening of the HCC bending angle decreases r_2(CC) and increases r_3(CN) in HCCN.

The variation of the potential energy along the MEP for α, β, and τ is displayed in Figure 3. The barrier to linearity for HCC and CCN is calculated to be 287 and 84 cm^{-1} along the respective MEPs. The torsion barrier, i.e., the energy difference between the optimum cis and trans HCCN conformations, is 84 cm^{-1}. In Figure 3, we also show the one-dimensional cut, V^{cut}, of the PES along the angle α, which is obtained by freezing the other five coordinates at their equilibrium values. On V^{cut},

TABLE 4: Combination Bands Involving the Stretching ν_1 Vibration[a]

	HCCN			DCCN		
	this work	expt	ref	this work	expt	ref
$\nu_1+\nu_5^1$	3356.40	3355.504(2)	10	2500.26	2499.572(1)	9
	[43.73, 1.70]	[45.33, 2.76]	10	[37.18, −16.53]	[32.72, −19.11]	9
$\nu_1+\nu_5^1-\nu_5^1$	3227.44	3226.597(2)	6	2424.60	2424.727(1)	9
$\nu_1+2\nu_5^0$	3690.06			2750.61		
	[7.48]			[11.85]	[12.29]	9
$\nu_1+2\nu_5^0-2\nu_5^0$	3229.10			2432.68	2432.1316(11)	9
$\nu_1+2\nu_5^2$	3552.69			2623.67		
	[−2.68]	[24.68]	12	[−8.74]	[−5.07]	9
$\nu_1+2\nu_5^2-\nu_5^1$	3423.73	3420.6663(6)	12	2546.71	2544.7432(9)	12
$\nu_1+3\nu_5^3$	3809.80			2788.33		
$\nu_1+3\nu_5^3-2\nu_5^2$	3464.17	3460.9116(8)	12	2575.46	2573.4795(7)	12
$\nu_1+2\nu_5^2-2\nu_5^2$	3209.25	3207.8482(6)	12	2412.78	2411.636(3)	9
$\nu_1+\nu_4^1$	3673.97			2836.22		
	[5.41, −22.63]	[8.76, −23.32]	6	[9.03, −36.38]		
$\nu_1+\nu_4^1-\nu_4^1$	3243.95	3244.084(1)	6	2428.74		
$\nu_1+\nu_5^1-\nu_1$	109.01	108.85	12	62.96	63.20	12
$\nu_1+2\nu_5^2-\nu_1$	303.84	302.92	12	185.07	183.22	12
$\nu_1+3\nu_5^3-\nu_1$	558.77	555.98	12	347.76	345.06	12
$\nu_1+2\nu_5^0-\nu_1$	443.40			313.97		

[a] For more details, see Table 2.

TABLE 5: Bending Frequencies ν_5^{eff} (in cm^{-1}) of HCCN and DCCN for the Ground-State (gs), ν_1, ν_2, and ν_3[a]

	HCCN			DCCN		
	ν_5^{eff}	$V_{\text{eff}}^{\text{lin}}$	$\theta_1^{\min}$	ν_5^{eff}	$V_{\text{eff}}^{\text{lin}}$	$\theta_1^{\min}$
gs	129	257	148	76	274	150
ν_2	137	179	150	92	193	152
ν_3	116	323	147	59	333	149
ν_1	109	332	146	63	346	148

[a] The height of the barrier to linearity $V_{\text{eff}}^{\text{lin}}$ (in cm^{-1}) and the location of the minimum $\theta_1^{\min}$ (in deg) are additionally shown.

the arrangement with $\alpha = 180°$ is lying 528 cm^{-1} above the absolute minimum and is thus 241 cm^{-1} higher than the corresponding MEP value. A similar one-dimensional cut of the PES in the direction of β shows no noticeable deviation from the corresponding MEP.

3. Method for Rovibrational Calculations

In the bound state variational calculations for the rovibrational energies of H/DCCN, we have employed the orthogonal (diatom + diatom) internal vectors **R**, $\mathbf{d}_1$, $\mathbf{d}_2$ in the body-fixed formulation.[31] The vectors $\mathbf{d}_1$ and $\mathbf{d}_2$ are chosen to be the HC and CN bond distance vectors, whereas **R** is the vector joining the centers of mass of the HC and CN subunits. The internal vectors are parametrized in terms of the three distances R, d_1, and d_2, the two bending angles θ_1 and θ_2, and the dihedral angle χ, schematically shown in Figure 1b. The reduced masses μ_R, μ_{d_1}, and μ_{d_2} associated with **R**, $\mathbf{d}_1$, and $\mathbf{d}_2$ are given for HCCN explicitly by $\mu_{d_1} = m_H m_C/(m_H + m_C)$, $\mu_{d_2} = m_C m_N/(m_C + m_N)$, and $\mu_R = m_{HC} m_{CN}/M$, where m_A stands for the mass of the unit A and M for the overall mass of HCCN. The two-vector embedded body-fixed (BF) reference frame is chosen such that the z-axis of the BF is aligned with the vector **R** and the $z \wedge x$ BF plane is the plane spanned by **R** and $\mathbf{d}_1$.

The MR-ACPF PES minimum in terms of the (diatom + diatom) coordinates is given by $R^e = 3.845a_0$, $\theta_1^e = 149.6°$, $\theta_2^e = 2.31°$, and $\chi^e = 180°$, while $d_1^e = r_1^e$ and $d_2^e = r_3^e$.

For an entirely orthogonal set of the internal vectors, such as the (diatom + diatom) vectors of Figure 1b, the body-fixed expression of the kinetic energy operator $\hat{T}$ from ref 31 can be rewritten as a sum of several contributions

$$\hat{T} = \hat{T}_{\text{vib}} + \hat{T}_{\text{rot}} + \hat{T}_{\text{cv}} + \hat{T}_{\text{cr}} \tag{3}$$

where $\hat{T}_{\text{vib}}$ and $\hat{T}_{\text{rot}}$ stand for the vibrational and rotational parts. The term $\hat{T}_{\text{cv}}$ is Coriolis-like kinetic coupling in the vibrational angular subspace, whereas $\hat{T}_{\text{cr}}$ is Coriolis-like kinetic coupling between the rotation and vibrational angular motion. The four contributions are explicitly given by

$$\hat{T}_{\text{vib}} = \hat{T}_{\text{str}} + \hat{T}_{\text{bend}} \tag{4}$$

$$2\hat{T}_{\text{bend}} = f(R, d_2)\hat{l}_2^{\,2} - f(R, d_1)[\hbar^2(\partial^2_{\theta_1} + \cot\theta_1\partial_{\theta_1}) - (\hat{J}_z - \hat{l}_{2z})^2/\sin^2\theta_1] \tag{5}$$

$$2\hat{T}_{\text{rot}} = f_R[\hat{J}^2 - 2(\hat{J}_z - \hat{l}_{2z})^2] \tag{6}$$

$$\hat{T}_{\text{cv}} = f_R(-i\hbar\hat{l}_{2y}\partial_{\theta_1} + \cot\theta_1\hat{l}_{2x}\hat{l}_{2z}) \tag{7}$$

$$\hat{T}_{\text{cr}} = f_R[i\hbar\hat{J}_y\partial_{\theta_1} - \hat{J}_x\hat{l}_{2x} - \hat{J}_y\hat{l}_{2y} - \hat{J}_z\hat{l}_{2z} + \cot\theta_1(\hat{J}_x\hat{J}_z - \hat{J}_x\hat{l}_{2z} - \hat{l}_{2x}\hat{J}_z)] \tag{8}$$

where $\hat{J}$ is the angular momentum of the nuclear frame and $\hat{T}_{\text{str}} = \hat{T}_{\text{str}}(R) + \hat{T}_{\text{str}}(d_1) + \hat{T}_{\text{str}}(d_2)$ stands for the kinetic energy of the three stretching vibrations. The term $\hat{T}_{\text{cv}}$ affects only vibrational energies and may lead to vibrational l-type doubling/resonance effects. Rotational l-type doubling/resonance effects may arise from $\hat{T}_{\text{cr}}$.

In eqs 4−7, ∂_{θ_1} stands for $\partial/\partial\theta_1$, $\partial^2_{\theta_1}$ for $\partial^2/\partial\theta_1^2$, and f_R for $1/\mu_R R^2$. The function $f(R, d_i)$, defined as $1/\mu_R R^2 + 1/\mu_{d_i} d_i^2$, is the inverse of the reduced mass associated with the bending coordinate θ_i. The vibrational angular momentum operator associated with $\mathbf{d_2}$ is $\hat{\mathbf{l}}_2 = \hat{\mathbf{l}}_2(\theta_2,\chi)$. The body-fixed projections of $\hat{J}$ are $\hat{J}_x$, $\hat{J}_y$, $\hat{J}_z$.

The standard rotation-angular basis in the body-fixed formulation is given for tetratomic molecules by the following product[31]

$$\bar{P}_{l_1}^{\,|k-K|}(\cos\theta_1)Y_{l_2}^{\,k}(\cos\theta_2,\chi)|JKM\rangle \tag{9}$$

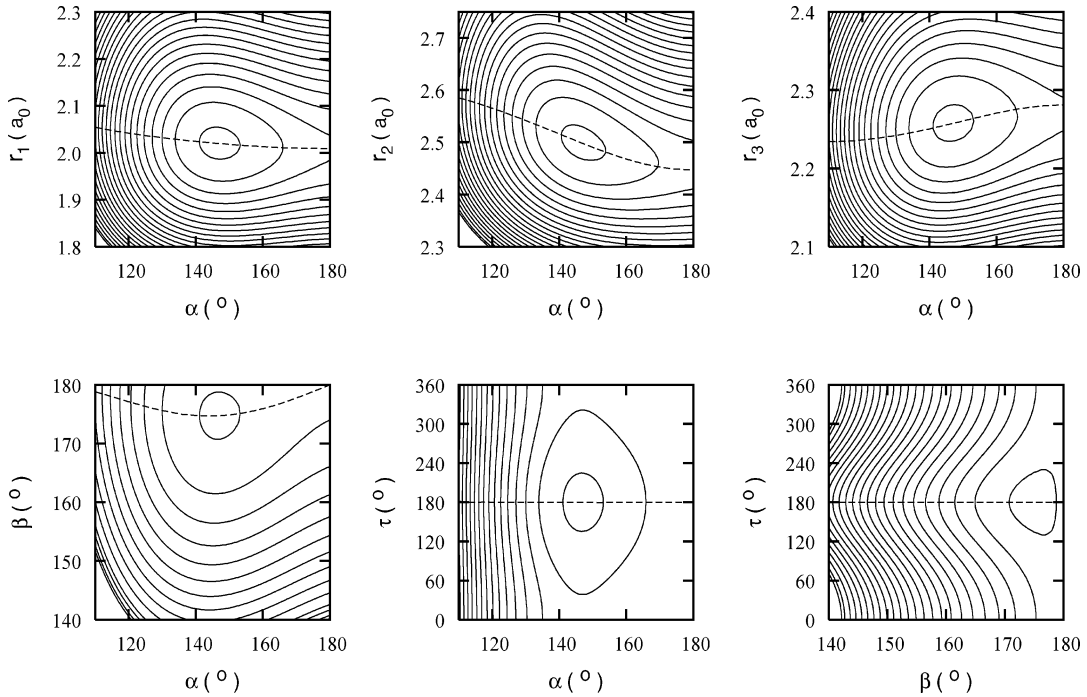

Figure 2. Two-dimensional contour plots of the six-dimensional MR-ACPF PES, obtained by freezing the remaining four coordinates at their equilibrium values. Contour lines are drawn in intervals of 250 cm^{-1} with the first contour placed at 50 cm^{-1}. The dashed lines show the variation of the internal coordinate shown on the *y*-axis along the minimum energy path for the coordinate displayed on the *x*-axis.

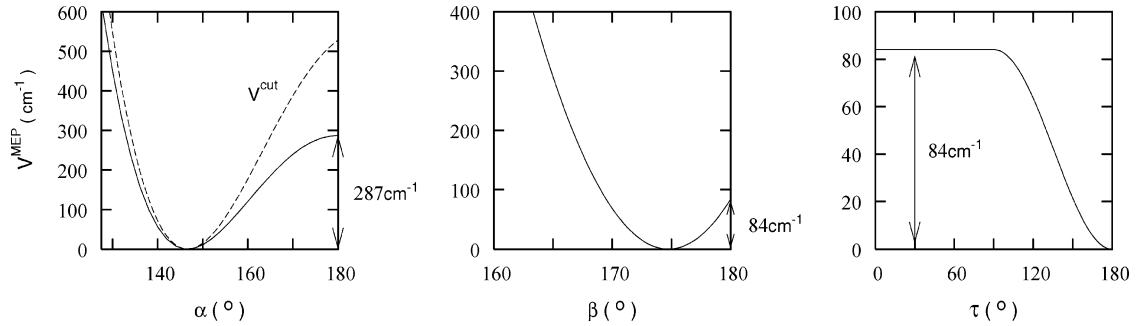

Figure 3. Minimum energy path (solid line) along the HCC angle α, the CCN angle β, and the torsion angle τ. The one-dimensional cut V^{cut} along α is given by the dashed line.

where $\bar{P}_l^k(\cos\theta)$ are normalized associated Legendre functions and $Y_{l_2}^k(\cos\theta_2,\chi)$ are spherical harmonics with the Condon−Shortley phase convention.[32] The quantum number of the projection of $\hat{\mathbf{l}}_2$ onto the *z*-axis of the BF is *k*. The symmetric top eigenfunctions[33] are denoted by $|JKM\rangle$, where *M* and *K* are the quantum numbers for the space-fixed *Z*-projection and the body-fixed *z*-projection of $\hat{\mathbf{J}}$, respectively. The action of the kinetic energy operator $\hat{T}$ of eq 3 on the basis functions of eq 9 can be solved analytically.[31]

The total rotational angular momentum *J*, its space-fixed projection *M*, and the parity *p* are strictly conserved quantum numbers for the eigenstates of a tetratomic molecule. For a given *J*, a parity-adapted angular basis can thus facilitate the computation. A detailed description of the parity-adapted rotation-angular basis functions employed in the present work can be found in ref 31.

In actual computations, the discrete variable representation (DVR) for the bending angles $\theta_1$and θ_2 is used together with the finite basis representation (FBR) of the dihedral angle χ, the eigenfunction basis in d_1, d_2, and the discretized Jacobi coordinate *R*. The DVR+FBR is combined with a sequential diagonalization/truncation scheme. This approach is termed DVR(+R)+FBR[34] and involves no dynamical approximation. In the DVR(+R)+FBR method, contributions to the rovibrational Hamiltonian are taken sequentially into account. After the inclusion of new term(s), the higher-dimensional Hamiltonian matrix is calculated and diagonalized, while the basis set is truncated by retaining only a preselected number of eigenvectors for subsequent computations. For chosen *K*, *k*, R_z and parity *p*, where R_z stands for a discrete point in *R*, the terms $\hat{T}_{\text{bend}} + \hat{T}_{\text{str}}(d_1) + \hat{T}_{\text{str}}(d_2)$, and $\hat{T}_{\text{rot}}$ are first considered together with the potential energy contribution diagonal in *k*. In the next step, the term $\hat{T}_{\text{cv}}$ is added along with the potential energy contribution nondiagonal in *k*, resulting in five-dimensional eigenvalue problems for each of the pairs (K, R_z). The inclusion of the kinetic energy in *R* leads to the formulation of six-mode eigenvalue problems for a fixed *K*. The final nine-dimensional rovibrational Hamiltonian matrix is constructed by including the term $\hat{T}_{\text{cr}}$ and is of relatively modest size owing to a very efficient contraction scheme of the DVR(+R)+FBR approach. At different stages of calculation, the Hamiltonian matrices are diagonalized by conventional dense matrix algorithms to give both eigenvalues and eigenfunctions.

A. Adiabatic Projection Scheme. The computational strategy of the DVR(+R)+FBR approach readily permits the construction of the adiabatic (zero-order) basis, consisting of eigenvectors computed in the adiabatic *R*-stretch approximation.

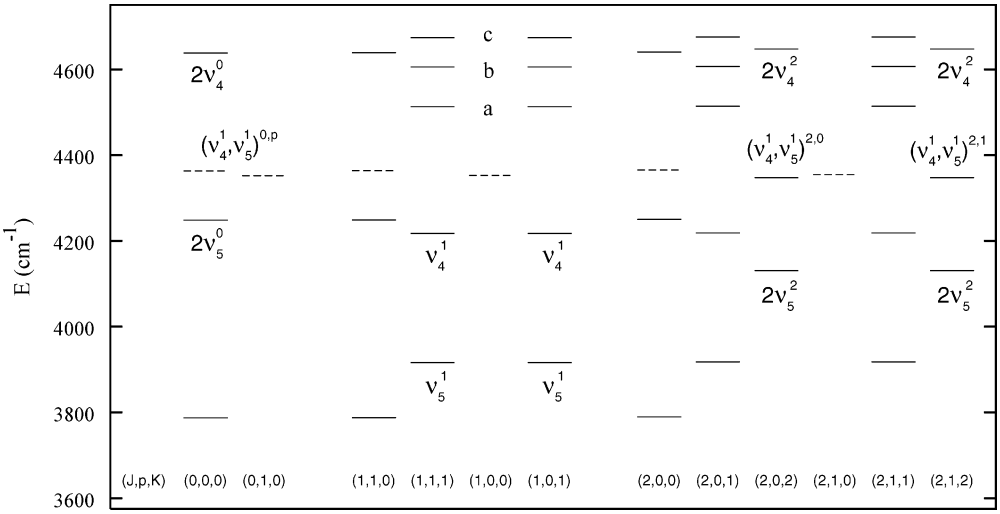

Figure 4. Low-lying states of HCCN calculated for total rotational angular momentum J and parity p. The quantum number assignments are made according to the linear molecular model. The quantum labels of the states denoted by a, b, and c are $3\nu_5^1$, $(\nu_4^1, 2\nu_5^2)^{1,p}$, and $(\nu_4^1, 2\nu_5^0)^{1,p}$, respectively. For the states shown, the quantum label K for the projection of $\hat{\mathbf{J}}$ on the body-fixed z-axis is essentially a good quantum number.

The five-mode eigenstates calculated for a grid of the discrete points R_z form adiabatic potentials V^i_{adi} for R. The stretching states $|\alpha\rangle$, adiabatically separated from the remaining five vibrational modes, can be obtained for the ith five-mode state by employing the adiabatic Hamiltonian $\hat{H}^i_{\text{adi}} = \hat{H}^i_{\text{adi}}(R)$, consisting of the kinetic energy $\hat{T}_{\text{str}} = \hat{T}_{\text{str}}(R)$ and the adiabatic potential V^i_{adi}. To monitor the evaluation of the adiabatic representation within the DVR(+R)+FBR computational scheme, the quantum state character correlation scheme is used. The latter scheme was originally developed for the adiabatic torsion approximation and the DVR(6) approach.[35]

The adiabatic vectors $|\alpha, i) = |\alpha\rangle| i\rangle$ are used in the DVR(+R)+FBR for the calculation of adiabatic expansions of numerically exact wave functions $| n\rangle$

$$|n\rangle = \sum_{\alpha, i} C_{\alpha,i}{}^{n} |\alpha, i) \tag{10}$$

The latter expansion supplies a zero-order origin of $|n\rangle$ by locating the dominant adiabatic contribution among all $|\alpha, i)$, providing, thus, an important foundation for quantum number assignments. The adiabatic projection of eq 10 is easily extended to include also the $J \neq 0$ situation.

B. Numerical Details. The numerical parameters used to compute the rovibrational energy levels of H/DCCN for $J = 0-4$ by means of the DVR(+R)+FBR are summarized here. The pointwise representation of the Jacobi distance R is obtained in the spirit of the potential optimized DVR method of Echave and Clary.[36] For HCCN, we used 12 discrete R_z points distributed nonevenly between $3.54a_0$ and $4.43a_0$. Three eigenfunctions for d_1 and five eigenfunctions for d_2 were constructed for the reference potential determined by the equilibrium H/DCCN geometry. The maximum value $k^{\max}$ for the projection quantum number k was 5 in $J = 0$ and 9 in $J = 4$ calculations. The integrals over the dihedral angle χ were solved by means of Gauss−Chebyshev quadrature of order 11. For the bending angles, Gauss−Legendre DVR points were used, determined from $P^k_{l_1^{\max}}$ of $k = 0, 1, \cdots, k^{\max}$ with $l_1^{\max}$ of 35 for θ_1 and $l_2^{\max}$ of 95 for θ_2. The Gauss−Legendre DVR set was truncated, keeping only the points distributed between 90 and 180° for θ_1 and between 0 and 40° for θ_2. The primary basis included 347400 functions for $J = 0$ and 3495960 for $J = 4$. The truncation of the basis set was made with the help of the cutoff parameters $N_k{}^{\max}$, $N_z{}^{\max}$, and $N_K{}^{\max}$, which give the number of eigenvectors to be saved after the diagonalization of the (K, R_z, k)-blocks, (K, R_z)-blocks, and K-blocks, respectively. The parameters $N_k{}^{\max}$, $N_R{}^{\max}$, $N_K{}^{\max}$ were chosen to be 150, 800, and 500, respectively. The size of the six-dimensional matrices of the K-blocks was thus 9600. The size of the final rovibrational Hamiltonian matrix was 1000, 1500, 2000, and 2500 for $J = 1, 2, 3, 4$, respectively.

4. Results

Selected results obtained for $J = 0-4$ by means of the DVR(+R)+FBR method and the MR-ACPF PES are shown in Tables 2−5 and Figures 4−7. In these tables, the level energies are given relative to the ground vibrational state, calculated to be 3787.357 cm^{-1} for HCCN and 3289.913 cm^{-1} for DCCN.

A. Quantum State Labels. Following the conventional linear molecule notation, the state assignments can be made in terms of ν_1, ν_2, ν_3, $\nu_4^{l_4}$, and $\nu_5^{l_5}$. The mode labels ν_1, ν_2, ν_3, ν_4, and ν_5 refer respectively to CH stretch, CN stretch, CC stretch, CCN bend, and HCC bend, whereas l_4, l_5 denote the vibrational angular momentum quantum numbers. The permitted values of l_i are v_i, $v_i - 2$, $v_i - 4$, ..., $-v_i$ for $i = 4, 5$.

Since K, $k \geq 0$ holds in the parity-adapted formulation,[31] we employ in the present work the quantum label $(v_4\nu_4^{|l_4|}, v_5\nu_5^{|l_5|})^{K,p}$, where p stands for parity ($p = 0$ for even parity and $p = 1$ for odd parity). In the body-fixed formulation used here, l_5 correlates to the projection quantum number k. Angular momentum conservation additionally restricts l_4, l_5 to $l_4 + l_5 = l = K \leq J$, as seen in eq 9 and ref 31. For quantum states given by $v_4 = 0$, we use the label $v_5\nu_5^K$, and similar for the $v_5 = 0$ situation.

The low-lying rovibrational states of HCCN calculated for $J = 0$, 1, and 2 and both parities are found in Figure 4. One may note that the levels ν_4^1 and ν_5^1 occur only for $J \geq 1$, whereas the states $2\nu_5^2$, $2\nu_4^2$, and $(\nu_4^1,\nu_5^1)^{2,p}$ become accessible for $J \geq 2$. The two $K = 0$ levels shown by the dashed lines in Figure 4 are assigned $(\nu_4^1,\nu_5^1)^{0,p}$ in the notation used here or $\nu_4^{\pm1} + \nu_5^{\mp1}$. The alternative assignment for the two $K = 2$ levels $(\nu_4^1,\nu_5^1)^{2,p}$ of Figure 4 is $\nu_4^{\pm1} + \nu_5^{\pm1}$.

In the bent molecule notation, the levels $2\nu_5^0$, (ν_4^1,ν_5^1),^{0,0} and $(\nu_4^1,\nu_5^1)^{0,1}$ are respectively ν_5^b, ν_4^b, and ν_6^b, whereas ν_5^1 and $2\nu_5^2$ correlate with the $K = 1$ and $K = 2$ (a-type) transitions from

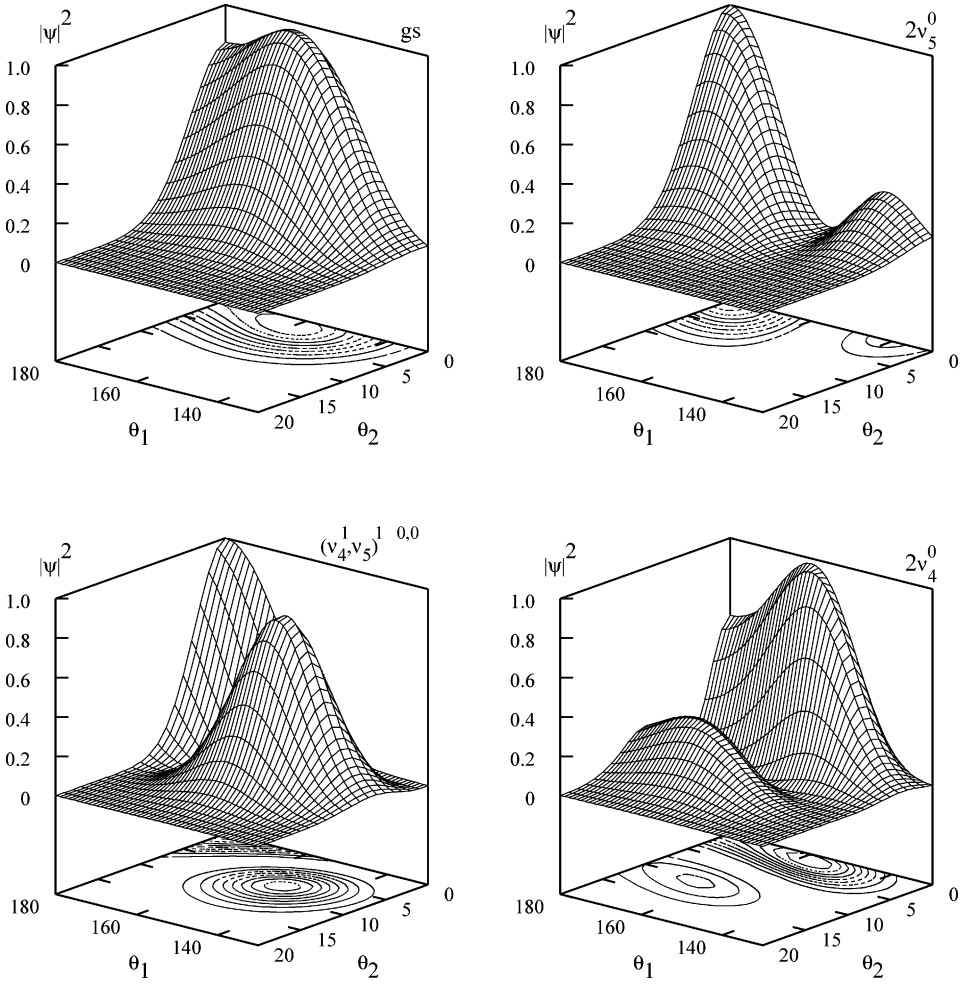

Figure 5. Wave function probability amplitudes for the ground vibrational state (gs), $2\nu_5^0$, $(\nu_4^1,\nu_5^1)^{0,0}$ and $2\nu_4^0$ of HCCN for $J = 0$. The remaining four coordinates are kept constant at their equilibrium values. The contours seen in the (θ_1,θ_2) plane show where the probability amplitude takes 10%, 20%, 30%, 40%, 50%, 60%, 70%, 80%, 90% of its maximum value.

the ground state. The levels assigned ν_4^1 in Figure 4 are, however, not easy to interpret by means of the bent molecular model.

The two-dimensional (θ_1,θ_2) cuts of the wave function probability amplitudes for the ground vibrational state, $2\nu_5^0$, $(\nu_4^1,\nu_5^1)^{0,0}$ and $2\nu_4^0$ of HCCN are shown in Figure 5. The well-defined nodal patterns seen for $2\nu_5^0$ and $2\nu_4^0$ in Figure 5 clearly imply the excitation of the θ_1 bending motion in $2\nu_5^0$ and the excitation of the θ_2 bending motion in $2\nu_4^0$, confirming the linear molecule convention for HCCN.

A striking feature in Figure 5 is a large wave function amplitude seen at the linear geometry, $\theta_1 = \pi$, even in the ground vibrational state. This property is also visible in Figure 6, where the wave function probability amplitude integrated over R, d_1, d_3, θ_2, χ and three Euler angles are shown for the ground vibrational state, ν_5^1, $2\nu_5^0$, $3\nu_5^1$, and $4\nu_5^0$. Although the ground vibrational state at 3787 cm^{-1} lies ≈90 cm^{-1} below the barrier to linearity, the ground-state wave function amplitude differs significantly from zero at $\theta_1 = \pi$. For the levels with $l_5 = 1$, the wave function amplitude at $\theta_1 = \pi$ is strictly zero as a consequence of the rotational symmetry, Figure 6 and eq 9. The states with $l_5 \neq 0$ exceed the barrier to linearity.

The vibrationally averaged bending amplitude $\langle\theta_i - \theta_i^e\rangle$ is calculated as $\arccos[\langle\cos(\theta_i - \theta_i^e)\rangle]$. For the ground vibrational state, $2\nu_5^0$, $(\nu_4^1,\nu_5^1)^{0,0}$ and $2\nu_4^0$ of Figure 5, the amplitude $\langle\theta_1 - \theta_1^e\rangle$ describing the quasilinear mode is calculated to be 11.4, 16.0, 10.6, and 12.0°, respectively. For $\langle\theta_2 - \theta_2^e\rangle$, we obtained 4.2, 4.2, 6.3, and 8.0°.

B. Fundamental Transitions. The fundamental transitions of HCCN and DCCN are summarized in Table 2. The MR-ACPF PES, adjusted to reproduce experimental wavenumbers for ν_5^1 and ν_1 of HCCN (section 2), provides a good description of ν_5 and ν_1 also for DCCN. As seen in Table 2, the ν_1 and ν_5 frequencies calculated for DCCN differ by +0.27 and +0.81 cm^{-1} from the high-resolution spectroscopic results of Sun et al.[9]

So far, no high-resolution spectroscopic study has been reported for the ν_3 and ν_4 vibrations of either HCCN or DCCN. Dendramis and Leroi[3] derived from matrix isolation infrared spectra five fundamental transitions for various isotopically substituted forms. McCarthy et al.[7] and Morter et al.[6] estimated the transition energies of ν_4 and ν_5 from relative intensity measurements in the microwave and infrared region, respectively.

Miller et al.[8] recorded the high-resolution infrared spectrum of HCCN in the region of the ν_2 stretching fundamental and found six separate vibrational bands. However, no vibrational identification could be made. Fermi resonance between ν_2 and $\nu_3 + (\nu_4^1,\nu_5^1)^{0,0}$ was suggested in ref 8 as a probable intensity borrowing mechanism in the region of ν_2.

In the present work, the energy spectra calculated for HCCN and DCCN are studied in great detail with the help of the adiabatic expansions of eq 10. This analysis led to the

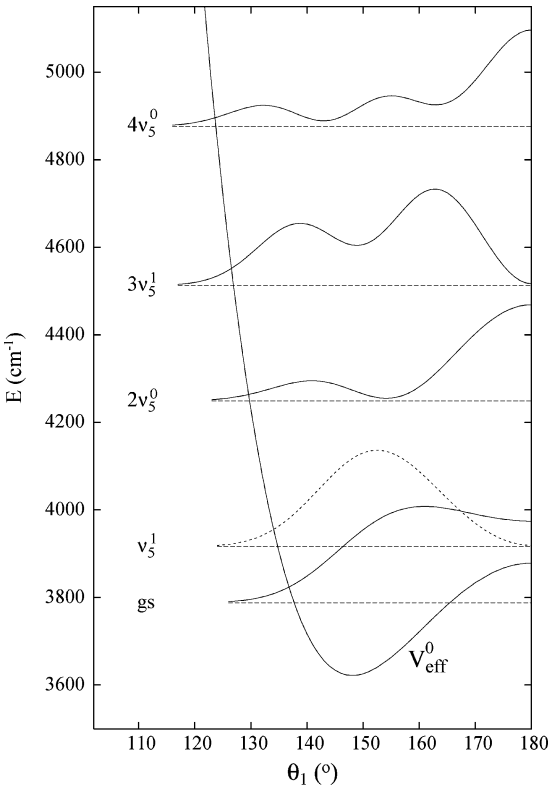

Figure 6. Wave function probability amplitudes integrated over the five internal coordinates R, d_1, d_2,θ_2,χ and three Euler angles for the ground vibrational state (*gs*), ν_5^1, $2\nu_5^0$, $3\nu_5^1$, and $4\nu_5^0$ of HCCN. The levels shown are calculated for $J = 1$ and $p = 1$. The effective ground-state potential energy profile along θ_1 is denoted by V_{eff}^0. The horizontal lines indicate the level energy.

identification of several resonances involving the fundamental stretching ν_2 and ν_3 vibrations. For HCCN, we have

$$|\nu_2\rangle \approx 0.799|\,0,\,9) - 0.439|\,1,\,2) \qquad (11)$$

$$|\nu_3 + (\nu_4^1,\nu_5^1)^{0,\,0}\rangle \approx 0.534|\,0,\,9) + 0.725|\,1,\,2)$$

and

$$|\nu_3\rangle \approx -0.428|\,0,\,5) + 0.818|\,1,\,0) \qquad (12)$$

$$|(\nu_4^1,\,3\nu_5^1)^{0,\,0}\rangle \approx -0.803|\,0,\,5) - 0.447|\,1,\,0)$$

The HCCN levels ν_2, $\nu_3 + (\nu_4^1,\nu_5^1)$,^{0,0} ν_3, and $(\nu_4^1,\,3\nu_5^1)^{0,0}$ occur at 1733.7, 1759.2, 1178.6, and 1185.8 cm^{-1}, respectively. The ν_2 state of DCCN displays no resonance mixing. For ν_3 of DCCN, we obtain

$$|(2\nu_4^0,\,2\nu_5^0)^{0,\,0}\rangle \approx 0.715|\,0,\,7) - 0.567|\,1,\,0) \qquad (13)$$

$$|\nu_3\rangle \approx 0.560|\,0,\,7) + 0.720|\,1,\,0)$$

where $(2\nu_4^0,\,2\nu_5^0)^{0,0}$ and ν_3 lie respectively at 1131.2 and 1150.6 cm^{-1}.

The adiabatic projections of eqs 11−13 are given in terms of the two dominant components, providing at least 81% of the full-dimensional wave function. For the zero-order vectors, we employ the notation used by the code, where $|\alpha,\,i)$ stands for the adiabatic level with α quanta in the stretching (R) vibration and i quanta in the five-mode vibration, as described in section 3.1.

Adiabatic projection methods are useful for quantitative studies on separability of internal molecular motions and for making quantum number assignments to the calculated full-dimensional rovibrational states. The adiabatic (zero-order) basis is, however, coordinate dependent. To verify eqs 11−13, we studied several other orthogonal (Jacobi type) descriptions and found that the levels ν_2 and ν_3 occur as zero-order mixtures also for Jacobi type coordinates. These test calculations led additionally to the conclusion that internal motion of HCCN is most separable in the (diatom + diatom) description of Figure 1b.

C. Transitions Involving the Bending ν_5 and ν_4 and Stretching ν_1 Vibrations. The transitions involving the bending ν_5 and ν_4 vibrations are summarized in Table 3, whereas Table 4 displays the transitions involving the stretching ν_1 vibration. The level energies in Tables 3 and 4 are in excellent agreement with high-resolution spectroscopic data of refs 6, 9, 10, and 12, showing a maximum deviation of +3.3 cm^{-1} for the combination band $\nu_1 + 3\nu_5^3 - 2\nu_5^2$ calculated at 3464 cm^{-1} for HCCN. One may note that in Table 4 we also list the energies $\nu_1 + n\nu_5^{\pm n} - \nu_1$ (n = 1, 2, 3), which are obtained in the semirigid bender calculations of Hung et al.[12]

The energy levels of the pure ν_4 and pure ν_5 bending vibrations of HCCN are graphically presented in Figure 7. The states of ν_4 follow in particular closely the energy pattern of the two-dimensional (anharmonic) oscillator.

To quantify the degree of quasilinearity of molecular vibrations, Yamada and Winnewisser[37] introduced the parameter γ_0, given by

$$\gamma_0 = 1 - 4[E(\nu_i^1) - E_0]/[E(2\nu_i^0) - E_0] \qquad (14)$$

Our results from Tables 2 and 3 give for the quasilinear ν_5 bending mode γ_0 of −0.12 for HCCN and of +0.05 for DCCN. On the other hand, we obtain γ_0 of −1.02 and −0.95 for the ν_4 of HCCN and DCCN, respectively, as expected for a degenerate bending mode in well-behaved linear molecules.[37]

In Figure 7, the states with $l_i \neq 0$ are doubly degenerate. Pronounced l-type splitting is, however, found only for the $K = 1$ states. For ν_5^1 and ν_4^1 of HCCN, the l-type doubling constant q_v is determined to be 40.1 and 27.6 MHz, which compare well to 40.6 and 27.9 MHz predicted by McCarthy et al.[7] For the ν_5^1 and ν_4^1 states of DCCN, the calculated q_v values of 49.9 and 35.6 MHz agree within 0.8 MHz with the experimental data[7] of 50.6 and 34.8 MHz. For the states $\nu_1 + \nu_5$, we obtained q_v of 42 MHz for HCCN and of 54 MHz for DCCN, which should be compared to q_v of 44 and 52 MHz estimated by Morter et al.[6] and Sun et al.[9]

As clearly seen in Figure 7, the level separation between $\upsilon_4\nu_4^{l_0}$ and $\upsilon_4\nu_4^{\upsilon_4}$ is much smaller than the separation between $\upsilon_5\nu_5^{l_0}$ and $\upsilon_5\nu_5^{\upsilon_5}$, where $l_0 = 0$ for υ_i even and $l_0 = 1$ for υ_i odd. For HCCN and DCCN, the level $2\nu_5^0$, e.g., lies 118 and 108 cm^{-1} above $2\nu_5^2$, respectively. An interesting difference between HCCN and DCCN is found in the ordering of the $2\nu_4^0$ and $2\nu_4^2$ states, Table 3. Whereas the levels $2\nu_4^{l_4}$ of HCCN show the expected ordering with the level $2\nu_4^0$ being 9 cm^{-1} below $2\nu_4^2$, the opposite is found for DCCN. In the latter case, the level $2\nu_4^0$ is 16 cm^{-1} above $2\nu_4^2$,

The bending HCC frequency obtained for four different stretching excitations are found in Table 5. The effective frequencies ν_5^{eff} are calculated as $E_{\nu_i+\nu_5} - E_{\nu_i}$ using the ($J = 1$, $p = 1$) values. As seen in Table 5, the excitation of ν_1 and ν_3 lowers ν_5^{eff} of HCCN approximately by 20 and 13 cm^{-1} and

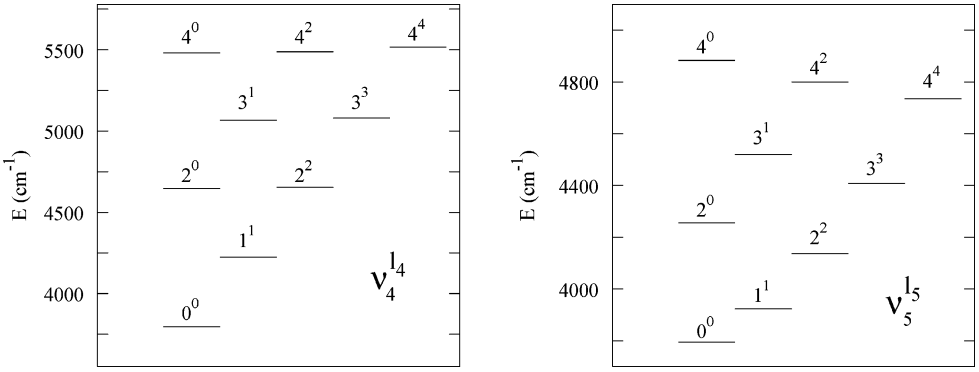

Figure 7. Energy levels of the pure ν_4 (left) and pure ν_5 (right) bending vibrations of HCCN, obtained for $J = 4$. One may note that the levels associated with $l_i \neq 0$ are doubly degenerate.

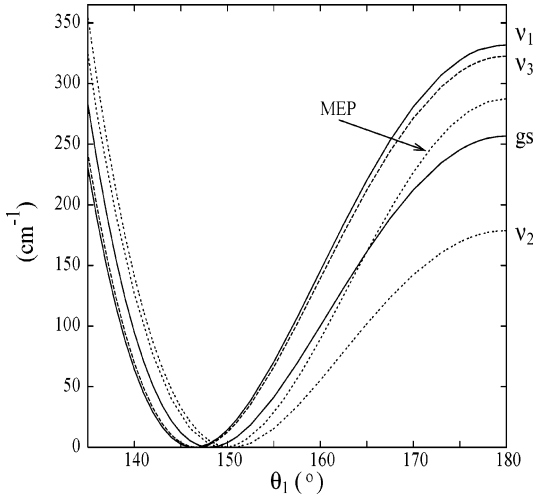

Figure 8. Effective potential energy profiles and the minimum energy path along the angle θ_1. For the purpose of comparison, each of the curves shown is measured relative to its minimum. The minimum energy path is denoted by MEP.

ν_5^{eff} of DCCN by 13 and 17 cm^{-1}, yielding changes up to 22%. On the other hand, ν_5^{eff} increases by 12 and 16 cm^{-1} upon excitation of ν_2 in HCCN and DCCN, respectively.

To gain a more general insight into the dynamics of the quasilinear ν_5 mode, we have also carried out detailed investigations of effective (adiabatic) potential energy profiles along the angle θ_1. For various excitations of other vibrational modes, the effective bending profiles were calculated in the spirit of the DVR(+R)+FBR strategy (section 3) by solving five-dimensional eigenvalue problems for a chosen θ_1 grid.

The effective θ_1 profiles obtained for the five-mode ground state, ν_1, ν_2, and ν_3 are depicted in Figure 8, whereas the height of the barrier to linearity, $V_{\text{eff}}^{\text{lin}}$, and the location of the minimum, θ_1^{min}, are presented in Table 5. As seen there, the height of the barrier to linearity on the five-mode ground-state profile is 30 cm^{-1} lower than the corresponding MEP value of 287 cm^{-1}. Upon excitation of ν_1 and ν_3, the barrier to linearity increases by 75 and 66 cm^{-1} for HCCN and by 72 and 59 cm^{-1} for DCCN relative to the ground-state value. At the same time, ν_2 excitation introduces lowering of $V_{\text{eff}}^{\text{lin}}$ by 78 cm^{-1} for HCCN and by 81 cm^{-1} for DCCN. According to Table 5, the effective bending frequency ν_5^{eff} nicely correlates with the effective barrier height $V_{\text{eff}}^{\text{lin}}$, i.e., the higher the barrier to linearity, the lower the effective bending frequency.

D. Rotational constants. In addition to the transition energies, Tables 2-4 also give the difference $\Delta B_{\text{v}} = B_0 - B_{\text{v}}$ between the ground-state rotational constant B_0 and the effective rotational constant B_{v} for the vibrational state v. The B_{v} values were determined by a least-squares fit of the calculated rovibrational energies to the following approximate expression

$$E_{\text{v}} = T_{\text{v}} + B_{\text{v}}J(J+1) \tag{15}$$

where T_{v} stands for the term energy.

The ground-state rotational constant B_0 is calculated to be 0.364872 cm^{-1} for HCCN and 0.329029 cm^{-1} for DCCN. They are 0.0016 and 0.0014 cm^{-1} smaller than the experimental values of 0.366465 and 0.330441 cm^{-1} derived from the millimeter spectra.[7] On the other hand, the theoretical results of Koput,[21] which read 0.367468 and 0.331676 cm^{-1}, overestimate B_0 by 0.0010 and 0.0012 cm^{-1}. One may also note that the equilibrium parameters (r_1^{e}, r_2^{e}, r_3^{e},α^{e},β^{e}) obtained here (section 2.2) differ by (0.0a_0, 0.011a_0, $-$0.016a_0, $-$1.7°, 0.7°) from the best estimate of Koput (2.020a_0, 2.510a_0, 2.241a_0, 144.9°, 175.4°) determined at the CCSD(T) level of theory.

The ΔB_{v} calculated for the fundamental transitions in Table 2 agree remarkably well (within 1.5 MHz) with the experimental values[3,6−9,11] for both HCCN and DCCN. Equally good agreement is also found for ν_5^1, $2\nu_5^2$, and $3\nu_5^3$ of DCCN in Tables 2 and 3. In the case of HCCN, the experimental and theoretical rotational constants for ν_5^1, $2\nu_5^2$, and $3\nu_5^3$ exhibit, however, different trends. While the experimental rotational constants[7] are nearly constant, our results in Table 3 for $2\nu_5^2$ and $3\nu_5^3$ of HCCN show rather prominent changes of ΔB_{v} with the l_5 excitation. Similar behavior is consequently seen for the state $\nu_1 + 2\nu_5^2$ in Table 4.

McCarthy et al.[7] also reported three $l = 0$ states at 435, 525, and 540 cm^{-1} for HCCN and one $l = 0$ state at 311 cm^{-1} for DCCN, each possessing a rotational constant somewhat larger than the ground-state B value, Table 3. Making use of the ΔB_{v} computed in the present work, the observed $l = 0$ states of HCCN are readily assigned $2\nu_5^0$, $(\nu_4^1,\nu_5^1)^{,0,1}$ and $(\nu_4^1,\nu_5^1)^{,0,0}$ while the $l = 0$ state of DCCN is labeled $2\nu_5^0$. For these four states, the calculated and experimental ΔB_{v} results agree to better than 4 MHz in Table 3.

5. Summary

In this paper, we have presented a detailed study of the rovibrational energy spectra of HCCN and its isotopomer DCCN. For the ground electronic state we first developed a six-dimensional MR-ACPF potential energy surface, which is subsequently adjusted to give best agreement with experimental data for ν_1 and ν_5 of HCCN. Quantum mechanical calculations were carried out for total rotational angular momentum $J = 0-4$ using the DVR(+R)+FBR method. In addition to the

transition energies, our study also includes the determination of spectroscopic parameters, such as effective rotational constants and *l*-type doubling constants.

The rovibrational energy levels of both HCCN and DCCN are studied in great detail by means of vibrationally averaged geometries and adiabatic projection methods. Resonance interaction of the ν_2 stretching mode with $\nu_3 + (\nu_4^1,\nu_5^1)^{0,0}$ is found in HCCN, whereas the ν_3 stretching mode of DCCN is coupled with $(2\nu_4^0, 2\nu_5^0)^{.0,0}$ To gain a more general insight into the dynamics of the quasilinear ν_5 bending mode, the effective (adiabatic) energy profiles along θ_1 have been calculated for various five-mode excitations. For both HCCN and DCCN, we have found a clear increase in the height of the effective barrier to linearity for the excited ν_1 and ν_3, resulting in the lower effective ν_5 bending frequency. On the other hand, ν_2 excitation lowers the barrier to linearity and increases the effective ν_5 frequency.

Acknowledgment. This work has been supported by the Deutsche Forschungsgemeinschaft through SFB 357 (Molekulare Mechanismen unimolekularer Prozesse). Computer time was made available to M.M. through a grant from the John-von-Neumann Institut für Computing (NIC) at Forschungszentrum Jülich.

References and Notes

(1) Bernheim, R. A.; Kempf, R. J.; Humer, P. W.; Skell, P. S. *J. Chem. Phys.* **1964**, *41*, 1156.
(2) Wasserman, E.; Yager, W. A.; Kuck, V. J. *Chem. Phys. Lett.* **1970**, *7*, 409.
(3) Dendramis, A.; Leroi, G. E. *J. Chem. Phys.* **1977**, *66*, 4334.
(4) Saito, S.; Endo, Y.; Hirota, E. *J. Chem. Phys.* **1984**, *80*, 1427.
(5) Brown, F. X.; Saito, S.; Yamamoto, S. *J. Mol. Spectrosc.* **1990**, *143*, 203.
(6) Morter, C. L.; Farhat, S. K.; Curl, R. F. *Chem. Phys. Lett.* **1993**, *207*, 153.
(7) McCarthy, M. C.; Gottlieb, C. A.; Cooksy, A. L.; Thaddeus, P. *J. Chem. Phys.* **1995**, *103*, 7779.
(8) Miller, C. E.; Eckhoff, W. C.; Curl, R. F. *J. Mol. Struct.* **1995**, *352/353*, 435.
(9) Sun, F.; Kosterev, A.; Scott, G.; Litosh, V.; Curl, R. F. *J. Chem. Phys.* **1998**, *109*, 8851.
(10) Han, J.-X.; Hung, P. Y.; DeSain, J.; Jones, W. E.; Curl, R. F. *J. Mol. Spectrosc.* **1999**, *198*, 421.
(11) Allen, M. D.; Evenson, K. M.; Brown, J. M. *J. Mol. Spectrosc.* **2001**, *209*, 143.
(12) Hung, P. Y.; Sun, F.; Hunt, N. T.; Burns, L. A.; Curl, R. F. *J. Chem. Phys.* **2001**, *115*, 9331.
(13) Jones, W. E.; Sun, F.; Curl, R. F.; Evenson, K. M.; Brown, J. M. *Can. J. Phys.* **2001**, *79*, 389.
(14) Nimlos, M. R.; Davico, G.; Geise, C. M.; Wenthold, P. G.; Lineberger, W. C.; Blanksby, S. J.; Hadad, C. M.; Petersson, G. A.; Ellison, G. B. *J. Chem. Phys.* **2002**, *117*, 4323.
(15) Zandler, M. A.; Goddard, J. D.; Schaefer, H. F., III. *J. Am. Chem. Soc.* **1979**, *101*, 1072.
(16) Kim, K. S.; Schaefer, H. F., III; Radom, L.; Pople, J. A.; Binkley, J. S. *J. Am. Chem. Soc.* **1983**, *105*, 4148.
(17) Rice, J. E.; Schaefer, H. F., III. *J. Chem. Phys.* **1987**, *86*, 7051.
(18) Malmquist, P. A.; Lindh, R.; Roos, B. O.; Roos, S. *Theo. Chim. Acta* **1988**, *73*, 155.
(19) Seidl, E. T.; Schaefer, H. F., III. *J. Chem. Phys.* **1992**, *96*, 4449.
(20) Francisco, J. S. *Chem. Phys. Lett.* **1994**, *230*, 372.
(21) Koput, J. *J. Phys. Chem. A* **2002**, *106*, 6183.
(22) Koput, J. *J. Phys. Chem. A* **2003**, *107*, 4717.
(23) Bunker, P. R.; Landsberg, B. M. *J. Mol. Spectrosc.* **1977**, *67*, 374.
(24) Gdanitz, R. J.; Ahlrichs, R. *Chem. Phys. Lett.* **1988**, *143*, 413.
(25) Cave, R. J.; Davidson, E. R. *J. Chem. Phys.* **1988**, *89*, 6798.
(26) Szalay, P. G.; Bartlett, R. J. *Chem. Phys. Lett.* **1993**, *214*, 481.
(27) Werner, H.-J.; Knowles, P. J. *Theo. Chim. Acta* **1990**, *78*, 175.
(28) MOLPRO is a package of ab initio programs designed by H.-J. Werner and P. J. Knowles. Amos, R. D.; Bernhardsson, A.; Berning, A.; Celani, P.; Cooper, D. L.; Deegan, M. J. O.; Dobbyn, A. J.; Eckert, F.; Hampel, C.; Hetzer, G.; Knowles, P. J.; Korona, T.; Lindh, R.; Lloyd, A. W.; McNicholas, S. J.; Manby, F. R.; Meyer, W.; Mura, M. E.; Nicklass, A.; Palmieri, P.; Pitzer, R.; Rauhut, G.; Schütz, M.; Schumann, U.; Stoll, H.; Stone, A. J.; Tarroni, R.; Thorsteinsson, T.; Werner, H.-J.
(29) Meyer, W.; Botschwina, P.; Burton, P. *J. Chem. Phys.* **1986**, *84*, 891.
(30) Mladenović, M. *J. Chem. Phys.* **2003**, *119*, 11513.
(31) Mladenović, M. *J. Chem. Phys.* **2000**, *112*, 1070.
(32) Arfken, G. *Mathematical Methods for Physicists*, 3rd ed.; Academic Press: New York, 1985.
(33) Zare, R. N. *Angular Momentum*; J. Wiley & Sons: New York, 1988.
(34) Mladenović, M. In *NIC Symposium 2001*; Rollnik, H., Wolf, D., Eds.; NIC Series 9; John von Neumann Institite for Computing: Jülich, Germany, 2002; pp 85−94.
(35) Mladenović, M. *Spectrochim. Acta, Part A* **2002**, *58*, 795.
(36) Echave, J.; Clary, D. C. *Chem. Phys. Lett.* **1992**, *190*, 225.
(37) Yamada, K.; Winnewisser, M. *Z. Naturforsch.* **1976**, *31A*, 139.